OPTICAL COMMUNICATION USING MICRO CORNER CUBE REFLECTORS

Patrick B. Chu*, Nanping R. Lo*, Erik C. Berg*, and Kristofer S. J. Pister*†
*Department of Electrical Engineering, University of California at Los Angeles,
Rm.54-148 Eng.IV, 405 Hilgard Ave, L.A., CA 90095-1594, U.S.A.
†Berkeley Sensor and Actuator Center, Department of EECS,
University of California at Berkeley, Berkeley, CA 94720, U.S.A.

ABSTRACT

Surface micromachined corner cube reflectors made of 250μm square hinged polysilicon plates have been demonstrated to transmit digital signals over a range of 2 meters by reflecting an interrogating 5mW laser. Measured reflectance ranges from 34% to 77% for different mirror designs. Divergence of light reflected by CCR ranges from 15-35mrad. The CCRs are electrostatically actuated with 10 to 20V. The highest data rate transmitted with a CCR is 1K bps.

INTRODUCTION

Zwirn proposed using a MEMS corner cube reflector to transmit digital signals by modulating the shape of the corner [1]. A corner cube reflector (CCR) has three mutually orthogonal reflective surfaces which form a concave corner. The mutual orthogonality insures that light which shines at the concave corner will be reflected directly back to the direction of the light source. By changing the shape of the CCR, the CCR can intermittently reflect light to its source direction, thereby communicating with an interrogating light source.

Fig. 1 shows one strategy of using a CCR as a communication link in a system. Consider a system which has a base station with a laser source and a remote station with an embedded sensor and a CCR. The remote station modulates the shape of the CCR according to the output of the sensor or some encrypted messages. The base station can shine a laser at the CCR of the remote station to read messages. In order to ignore signals from other light sources, the base station can also couple a frequency "signature" to the laser directed at the remote station and only read signals with the signature frequency.

Using CCRs as wireless communication links has several advantages including low power, small size, and low cost. The transmitter with a CCR may consume minimal power since it transmits data by reflecting external power. A corner cube reflector removes the need for precise angular alignment between the laser source and the CCR. The reflector may have dimensions in the sub-millimeter range. Batch fabrication technology for micromachining could also yield low cost systems. As a result, remote stations with micromachined sensors and CCR transmitters have the potential to be low powered, autonomous, small ($<< 1cm^3$) and inconspicuous, so that a large distribution of remote stations may be possible. The disadvantages of this communication approach include the need for a more complex base station and line of sight communication.

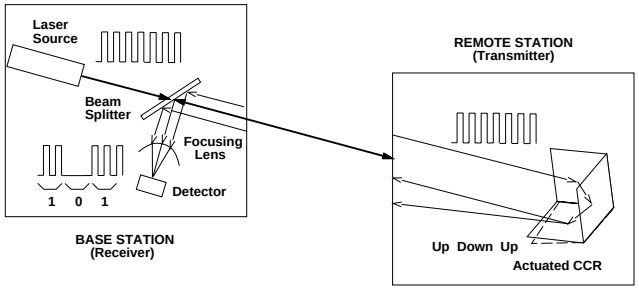

Fig. 1. Schematic diagram of a communication system using CCR as an optical wireless link.

Hinged polysilicon plates fabricated by surface micromachining can readily be used as micro mirrors and lenses [2], [3]. Earlier efforts in developing surface micromachined CCRs have been reported [4], [5]. In this paper, the operation principles of CCRs will be discussed. Some novel designs of microstructure components including an electrostatic actuator will be presented. Analysis and simulation of the electrostatic design will also be presented. The optical testing of fabricated CCRs and the realization of a communication system using a micro CCR as a communication link will be discussed.

CORNER CUBE REFLECTOR THEORY

An ideal corner cube reflector has 3 perfectly reflective, mutually orthogonal planar surfaces which together form a right angle concave corner. For a macro corner cube (which is much bigger in size than the incident beam spot size), it can be shown that an incident ray with direction $\hat{a} = (-a_x, -a_y, -a_z)$,with $\|\hat{a}\| = 1$ and $a_x, a_y, a_z \geq 0$, will be reflected back to the direction -$\hat{a}$ after it hits three mirror surfaces of the CCR (Fig. 2) [6], [7]. The light ray may also return to its source after two bounces or even one bounce if the appropriate component of the incident direction is zero. In this application, we are most interested in the three bounce case because it is most likely that the incident light has a direction with non-zero a_i. Since micro CCRs generally are assumed to be smaller in size than the incoming beam, we are also interested in the total effective area of the CCR.

Suppose an incident ray with direction (-a_x, -a_y, -a_z) struck the x-y mirror at $p_1 = (x_1, y_1, 0)$, and then the x-z mirror and the y-z mirror at $p_2 = (x_2, 0, z_2)$ and $p_3 = (0, y_3, z_3)$ respectively (Fig. 2). The following conditions can be derived for p_1 in terms of a_i's for the case where

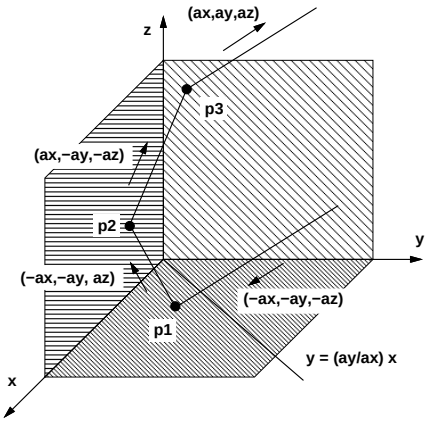

Fig. 2. This figure shows how the direction of an incident ray changes after hitting each mirror. Note that three successive reflections are not always possible depending on $p1$ and a_i's.

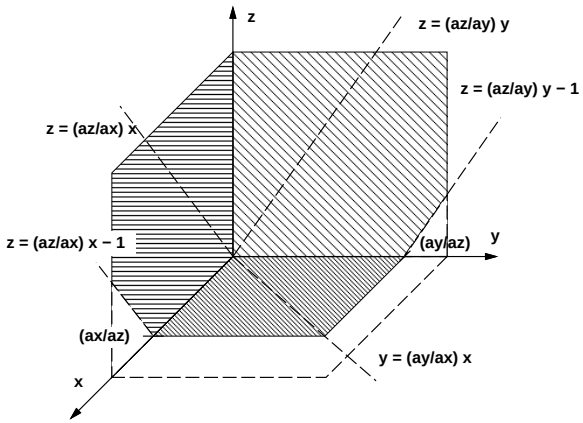

Fig. 3. Effective area of the CCR for an incident ray with direction $\hat{a} = (-a_x, -a_y, -a_z)$, $\|\hat{a}\| = 1$ and $a_x, a_y, a_z > 0$. The shading represents areas where the light ray must first strike in order to be reflected to $-\hat{a}$.

$0 < y_1 < (a_y/a_x)x_1 < 1$ and $a_y/a_x \leq 1$:

$$0 < y_1 < \frac{a_y}{a_z} < 1 \text{ and } 0 < x_1 < \frac{a_x}{a_z} < 1 \tag{1}$$

for all $a_i \geq 0$. An additional condition

$$y_1 > \frac{a_y}{a_x} x_1 - 1 \tag{2}$$

is found for $a_y/a_x > 1$. Similar conditions can be derived for the case where the light ray first hits the x-z mirror, followed by the y-z mirror and the x-z mirror.

We can conclude that a light ray of a given direction can be reflected back to its source only if it hits a particular region of the CCR. In other words, the effective area of a CCR changes as a function of the direction of an incident ray. Fig. 3 shows the area on the CCR where an an incident ray must first hit in order to be returned to the source. The effective area is the sum of each shaded area scaled by the corresponding direction cosine of the incident ray. The maximum effective area for a unit corner cube, thus, is $\sqrt{3}$. The direction which yields the largest effective area is $\frac{1}{\sqrt{3}}(1,1,1)$, although small deviation from this direction does not reduce the area significantly. For example, if the incident direction is within a solid angle of 0.3rad around $\frac{1}{\sqrt{3}}(1,1,1)$, the effective area is at least 50% of the maximum area, yielding less than 3dB of power loss. Given the effective area and the incident beam spot size, the reflected power may be estimated by the following equation:

$$P_{reflected} = P_{incident} \times \frac{A_{CCR}}{A_{spot}} \times R_{CCR} \tag{3}$$

The reflected power is also directly proportional to incident power, $P_{incident}$, and the reflectivity of the mirrors, R_{CCR}. R_{CCR} is equal to the product of the reflectivity of each of the three mirrors. The reflectivity is determined by the fabrication process. For polysilicon plates, the reported reflectance is 24% for 0.67μm wavelength [4]. For gold coated polysilicon plates, the reported reflectance is 0.93 for 1.3μm wavelength [8].

Orthogonality of the micro corner cube may also affect the effectiveness of a micro CCR, since the detected power from the CCR is proportional to the ratio of the sensor detector area and the area illuminated by the CCR. This area is defined divergence angle of the CCR and the communication distance. Atmospheric attenuation also may need to be taken into account if the communication distance is large.

MECHANICAL DESIGN OF CCR

We have designed micro CCRs which are surface micromachined via the MUMPS multiple layer polysilicon process offered by MCNC [9]. Mirrors made of polysilicon plates with a gold layer are rotated to a position normal to the substrate using microhinges and are locked in place with torsional spring locks (Fig. 4). A fabricated electrostatic CCR is shown in Fig. 5. Tenon and mortise are used to help align the two vertical plates. Torsional tie-downs are connected to the edges of the rotated plates to restrict potential offset due to slack in the hinges. Additional plates with slits are used to catch the edge of the mirror plates in order to improve orthogonality.

The mechanical misalignment for the vertical plates and the substrate is estimated to be less than 2.8mrad. The movable base mirror also has a misalignment of 6.7mrad due to a layout error. Both misalignments can be reduced to less than 1mrad in future designs. Due to the tensile gold layer on the polysilicon plate, the mirrors have measured radius of curvature ranging from 7 to 9.8mm, which gives a reflected light ray a divergence of 15 to 20mrad. The stresses estimated from these measurements using bending equations from composite materials [10] agreed with MCNC's measured values [9]. From optical experiments, measured divergence for laser light reflected by CCRs like the one in Fig. 5 ranges from 15mrad to 35mrad.

Mirror plates typically have linear dimensions of 250 to 300μm. No etch holes are put in the plates in order to create smooth mirror surfaces. As a result, the chips from MCNC must be etched in 49% HF for up to 15 minutes

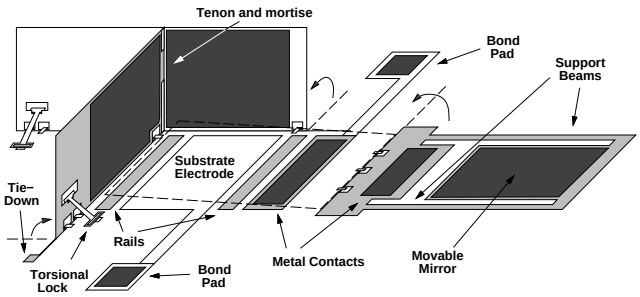

Fig. 4. One design of an electrostatically actuated corner cube for MCNC's polysilicon process. The base mirror of this CCR is formed by rotating a mirror plate to a tilted position above a substrate electrode.

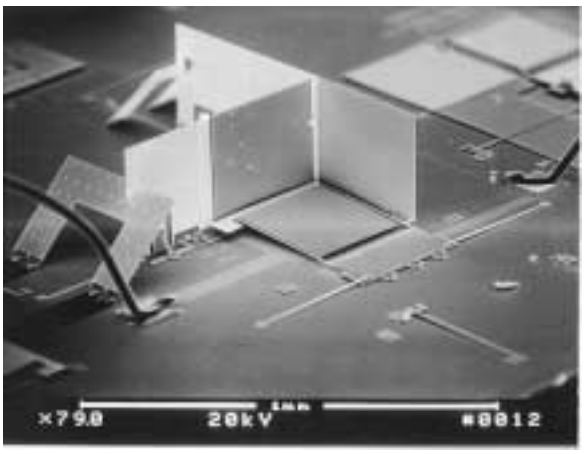

Fig. 5. An electrostatically actuated polysilicon CCR with a $250\mu m$ corner. The motion of the bottom plate modulates the reflection from the corner. The plate as shown is in an "up" position (the CCR is off).

in order to remove the sacrificial oxide layers. The long etch does not seem to cause any observable effect on the gold or polysilicon layers. Following the HF etch, the chips are rinsed in DI water and then isopropanol, which is then evaporated by placing the chips on a hot plate. Generally, this alcohol release method avoids stiction problems. Microstructures are then assembled using micro-manipulators at a microscope. Assembly is facilitated by the use of integrated microjacks (Fig. 6) [11].

The micro CCRs modulate the incident light by actuating a movable bottom mirror surface. The misalignment of one mirror of the CCR will deflect an incident light ray away from its source. The electrostatic CCR has a tilted bottom mirror surface which moves from an angled position ($\sim$ 3 degree) to a horizontal position when a voltage is applied across the tilted mirror and a substrate electrode (Fig. 7). The tilted mirror is made of a gold covered polysilicon plate which is rotated about several microhinges by a few degree less than 180 (Fig. 4) and is clamped down by beams (Fig. 6). A metal contact on the lower part of the rotated plate comes in contact with another metal contact on the substrate such that a voltage can be applied to the rotated plate. Two rails on the substrate help level the pulled-down mirror and prevent shorting between the con-

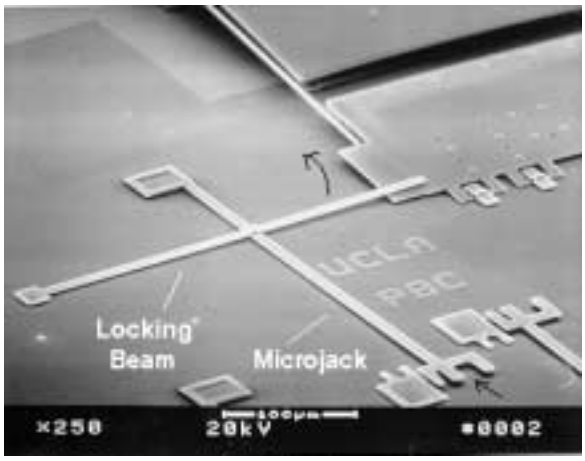

Fig. 6. Bent beams are used to prevent the rotated mirror from being disassembled. To assemble the tilted mirror, a probe applies an axial force to buckle the microjack, lifting the locking beam, the mirror is then rotated into position (Fig. 4), and the locking beam is lowered.

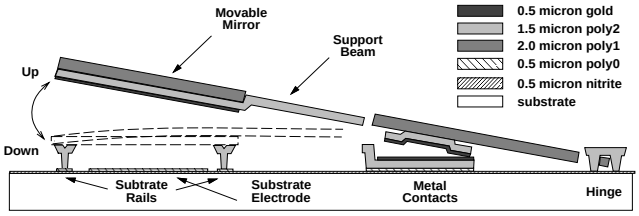

Fig. 7. Cross-section of the base plate actuator. Two rails on the substrate are used to help level the pulled-down mirror and to prevent short-circuiting across the actuator.

ductive mirror and the substrate electrode (Fig. 7).

The actuated mirror takes advantage of the nonlinearity and instability found in a typical spring-mass-electrostatic system such that the mirror can be pulled down with relatively low voltages. Typically, an actuation voltage of 10 to 15 volts is adequate to move the tilted mirror to a flat position. Estimated capacitance of the electrostatic actuator is < 0.2 pF. When the CCR is driven with 20 V and 10 kHz voltage input, the estimated power consumption of the actuator is $< 0.4\mu$W.

The flip-over actuated mirror design is not ideal because the polysilicon surface instead of the gold surface becomes the mirror. Fig. 8 shows an actuated mirror design with a gold reflective surface. It is made by a suspended plate which is pried up to an angled position with a sliding plate. Unfortunately, due to a layout flaw, electrical isolation is not properly provided, and the mirror becomes stuck after being pulled down. As a result, these CCRs can only be tested statically.

With a 4.7mW 670nm laser and a 3mm diameter spot size, the estimated total return power for an ideal corner is 97μW. The measured value for the CCR in Fig. 8 (with 3 gold front surface mirrors) is 75μW, corresponding to a R_{CCR} of 0.77 or a reflectivity of 0.92 for each gold mirror. The measured value for the CCR in Fig. 5 (with 2 gold and one poly front surface mirrors) is 33μW, corresponding to a R_{CCR} of 0.34. Assuming a reflectivity of 0.92 for each

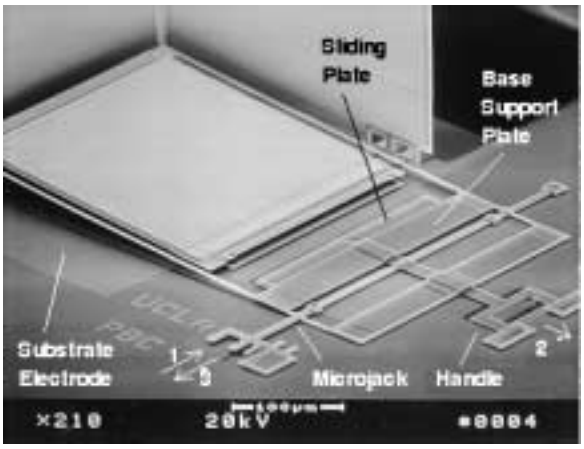

Fig. 8. A movable mirror with a gold front surface is assembled by 1) pushing on the microjack, 2) pulling on the handle to move the sliding plate underneath the base support plate of the mirror, and 3) releasing the microjack. The tilted mirror is then actuated like the design in Fig. 7.

gold mirror, the poly front surface mirror would have a reflectivity of 0.40.

ANALYSIS OF ELECTROSTATIC ACTUATOR

In order to predict the behavior of the nonlinear mirror system shown in Fig. 7, a lumped-element model has been used to simulate the system. The system equation is the following:

$$\begin{bmatrix} M_p\ddot{d} \\ I_p\ddot{\phi} \end{bmatrix} = \frac{V^2}{2}\frac{\epsilon W}{|\phi|}\begin{bmatrix} -\frac{L}{\delta}\left(\frac{2\sin\frac{|\phi|}{2}}{\delta-2L\sin\frac{|\phi|}{2}}\right) \\ \frac{1}{2\sin\frac{|\phi|}{2}}\left(\ln\left(\frac{\delta}{\delta-2L\sin\frac{|\phi|}{2}}\right)-\frac{2L\sin\frac{|\phi|}{2}}{\delta-2L\sin\frac{|\phi|}{2}}\right) \end{bmatrix} + \frac{EI}{l}\begin{bmatrix} \frac{12}{l^2} & -\frac{6}{l} \\ -\frac{6}{l} & 4 \end{bmatrix}\begin{bmatrix} d_0-d \\ \phi_0-\phi \end{bmatrix} - (1-0.6\frac{W}{L})(\frac{\mu W^3 L}{d^3})\begin{bmatrix} \dot{d} \\ (\frac{L}{2})^2\dot{\phi} \end{bmatrix} \quad (4)$$

where for $\phi \geq 0$,

$$\delta = d \quad (5)$$

and for $\phi < 0$,

$$\delta = d + 2L\sin\frac{|\phi|}{2} \quad (6)$$

E, ϵ, and μ represent Young's modulus of polysilicon, permittivity of free space, and viscosity of air. Other variables are explained in Table I.

The electrostatic actuator is modeled as a non-parallel capacitor. First, the electric field is found by solving Laplace's equation in polar coordinates as a function of the radial distance, neglecting the effect of fringing field. The capacitance is calculated using Gauss' law for electricity. The total energy is then calculated. The force applied to the support beams is calculated by taking a partial derivative of the total energy with respect to the vertical separation. The moment applied to the support beams is calculated by summing the product of the force due to a differential areas and the corresponding distances from the areas to the axis of rotation. The axis of rotation is along the points where the beams and the mirror are connected. The expressions of the electrostatic force and moment are shown as the first terms on the right side of the system equation.

The two support beams of the actuated mirror are modeled as ideal linear fixed-end rectangular beams with a force and moment load at the tip of the free end. The force and moment expressions are shown as the second term on the right side of the system equation. The damping force in the system is modeled by squeeze-film damping, and the damping moment is calculated by multiplying the damping force by the distance from the center of the mirror to the axis of rotation. The damping expressions are shown as the last term of the right side of the system equation.

The system equation in Eq. 4 describes the mirror's motion only when the mirror is not in contact with any rails on the substrate. To simulate the complete down-up cycle, one needs to recognize when one or more edges of the mirror collide with the rails and switch to a different model which takes into account of the applied force from the rails. The system equation is simulated with Matlab using Simulink and the Runge-Kutta fifth order method.

The model predicts a voltage at which the electrostatic

M_p	mass of the mirror	1.25	μg
I_p	moment of inertia of mirror	3.26×10^{-17}	kgm^2
W	width of mirror plate	250	μm
L	length of mirror plate	280	μm
I_b	moment of area of beams	2.25×10^{-24}	m^4
l	length of support beams	370	μm
V	applied voltage	0-20	V
d	gap distance (at the beams attachment)	–	μm
ϕ	angle between the plate and the substrate	–	deg
d_0	initial gap distance	20-30	μm
ϕ_0	initial plate angle	2-4	deg

TABLE I
EXPLANATION OF VARIABLES FOR THE SYSTEM EQUATION

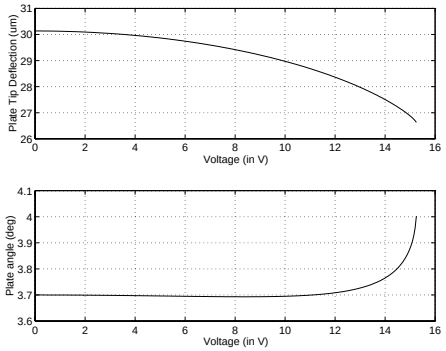

Fig. 9. Simulated deflection and angle of the bottom plate in Fig. 7 as a function of input voltages. Simulated pull-in voltage is $15.3V$.

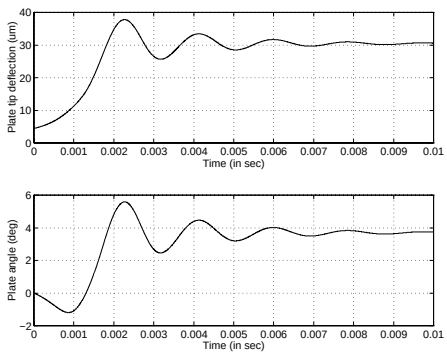

Fig. 10. Simulated positions of the bottom plate in Fig. 7 as it goes from the "down" position to the "up" position.

force will overwhelm the spring force, as seen in parallel-plate electrostatic systems [11]. Fig. 9 shows the simulated equilibrium positions of an actuator with voltage input from 0 to the predicted pull-in voltage of 15.3 V. The predicted voltage agrees well with experimentally observed pull-in voltages for this actuator, which cluster around 15 V. The increase in plate angle when the applied voltage approach 15V suggests that the unsupported mirror edge will first collide with a rail during a pull-down. This effect has also been observed.

Fig. 10 shows the simulated motion of the plate from a "pull-down" position to an idle position with no applied voltage. The natural frequency of the actuator is simulated to be 550Hz. Work is in progress to verify further the accuracy of this model.

DYNAMIC OPTICAL EXPERIMENT RESULTS

Optical bench tests in a dark room were performed on a number of fabricated devices. A 670nm He-Neon laser was shined at a modulated CCR through a beam splitter, and the returned light from the CCR was directed to a silicon PIN photo-diode with responsivity of about 0.45A/W for the wavelength of interest. A simple optical setup like this one does not provide precise information about the motion of the actuator due to the nonlinearity of the photo detector; however, it shows how the CCR will be seen by an interrogating laser source during a transmission in the absence of background noise.

Fig. 11 shows the raw signals (with no amplification) from the detector at the oscilloscope when the CCR in Fig. 5 is driven at different modulation frequencies. The square waves represent the input signal to the circuit which powered the CCR, where a low input activates the CCR. The high level of the detector waveforms correspond to increased intensity detected by the photo diode. Fig. 11 show that the detector waveforms change in shape and magnitude as the frequency changes.

At low frequencies, the change in detector output could be as high as 260mV (corresponding to about 0.5μW), with a relatively small DC offset of 50mV. Peaks are often observed before the rising and falling edges of the detector output. The source of these peaks is still unclear, although both Fig. 10 and Fig. 11 suggest that reflective transitions

Fig. 11. Raw output of photo detector for different CCR modulation frequencies. Direction of incident light is near (-1,-1,-1). The square wave represents the input signal which modulates the CCR, where a low input pulls down the movable mirror. Actuation voltage is 15V.

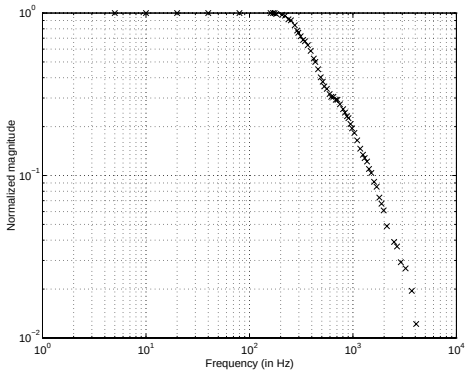

Fig. 12. Magnitude plot of the intensity change of the photo detector waveform as a function of CCR modulation frequency.

may occur more than once during each cycle. The rise time and delay of the rising edge have been observed to decrease with increased applied voltage (beyond the pull-in voltage). At high frequencies, the AC component of the detector waveform begins to decrease in amplitude while the voltage peak remains constant, indicating that the actuated mirror lacks time to move away from the pull-down position. Fig. 12 shows the AC magnitude change versus the frequency. The -3dB point occurred at 444Hz. It has also been observed that the detector waveform may change in intensity and shape depending on the direction of the incident light, yielding a different frequency magnitude plot (Fig. 13).

CCR AS A COMMUNICATION LINK

To demonstrate the operation of the fabricated micro CCR, a palm-size transmitter and a similar sized receiver have been built (Fig. 14). This transceiver can transmit either a periodic or an arbitrary digital signal from the transmitter to the receiver. The prototype transceiver system with the micro CCR operates in the arrangement shown in

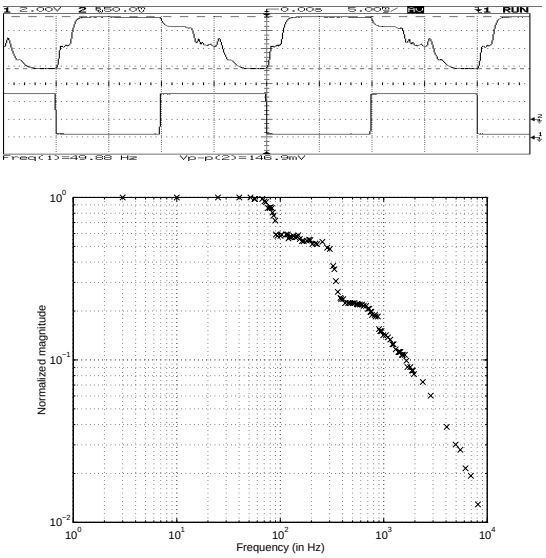

Fig. 13. Waveform and magnitude plots of the intensity change of the photo detector waveform as a function of CCR modulation frequency. The incident angle as well as the observed spot location are changed from Fig. 11. Actuation voltage is 18V.

Fig.1, where the receiver's laser beam is aimed at the CCR of the transmitter. A light emitting diode (LED) on the transmitter blinks according to the signal being transmitted, while another LED on the receiver blinks in synchrony when the receiver successfully detects the reflected signal.

The transmitter module is powered by a 9-volt battery. The chip with the micro CCR is glued and wire-bonded to a plastic substrate with copper bonding pads. The plastic substrate with the chip is stored inside a transparent petri dish to prevent damage to the CCR.

The receiver module contains a silicon PIN photo detector and a laser diode module from a commercially available laser pointer with wavelength of about 670 nm and a 1.7mW rms power output when modulated at 2 kHz (Fig. 1). The modulated signal returned from the CCR is high-pass filtered and amplified. The signal then goes through a threshold comparator to remove additional noise and is integrated to retrieve the actual transmitted data.

Free space communication across a distance of more than 1m under normal room light was demonstrated. With a CCR not covered with a petri dish lid, a distance of 2.1m has also been demonstrated. Highest observed communication rate transmitted and detected with the prototype is 1K bps. This proto-type system did not demonstrate the low-power and miniature-size advantages offered by micro CCRs; however, it provided proof of concept for the use of micro CCRs in free-space communication.

CONCLUSION

We have fabricated micro CCRs with a novel electrostatic actuator using surface micromachining. These CCRs have been demonstrated to function as a transmitter in an optical wireless transceiver system. Test results show that CCR with 77% reflection efficiency is feasible. Optical signals reflected from the CCR have been presented.

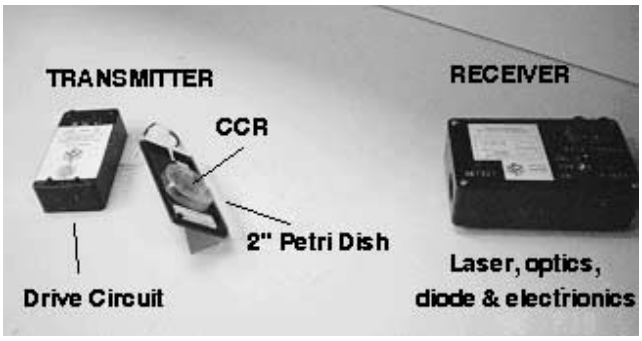

Fig. 14. Photo of prototype transmitter (on the left) and receiver (on the right). This device transmits up to 1K bps with a range of over $1m$ using the CCR shown in Fig. 5.

A non-linear model has also been designed for the CCR actuator to improve understanding of the behavior of the CCR. Future work will include modification of the CCR design to improve bandwidth, optical quality, and voltage requirement, designing a miniature low-power transmitter using the CCR, and evaluating its performance in a digital communication network.

ACKNOWLEDGMENTS

This work is supported by DARPA and NSF. The authors would like to thank Dr. Ming Wu and his group for sharing their equipments and facility, the staff at JPL's Micro Device Lab. particularly Dr. Howard Rockstad for many useful technical discussions, and Gisela Lin for the SEMs.

REFERENCES

[1] K. Brendley, and R. Steeb, "Military Applications of Microelectromechanical Systems," RAND report, RAND, Santa Monica, CA, 1993.

[2] L. Y. Lin, S. S. Lee, K. S. J. Pister, and M. C. Wu, "Three-dimensional micro-Fresnel optical elements fabricated by micromaching technique," Electronics Letters, vol. 30, no. 5, pp. 448-449, 1994.

[3] O. Solgaard, M. Daneman, N. C. Tien, A. Friedberger, R. S. Muller, and K. Y. Lau, "Micromachined alignment mirrors for active opto-electronics packaging," Conf. Lasers and Electro-Optics, Anaheim, CA, May 8-13, 1994, post-deadline paper CPD6.

[4] D. S. Gunawan, L-Y. Lin, K. S. J. Pister, "Micromachined corner cube reflectors as a communication link," *Sensors and Actuators A*, vol. A47, no. 1-3, pp. 580-583, 1995.

[5] J. H. Comtois, V. Bright, "Surface Micromachined Polysilicon," *Technical Digest, Solid State Sensors and Actuators Workshop*, Hilton Head, SC, 2-6 June, pp. 174-177, 1996.

[6] M. Rafalowski, "Determination of the working area for the corner-cube mirror system with variable angle of incident beam for interferometric applications," *Optica Applicata*, vol. 25, no. 2, pp. 141-8, 1995.

[7] M. S. Scholl, "Ray trace through a corner-cube retroreflector with complex reflection coefficients," *Journal of the Optical Society of America A*, vol. 12, no. 7, pp. 5394-7, 1995.

[8] S. S. Lee, L. -Y. Lin, M. C. Wu, "Realization of FDDI optical bypass switches using surface micromachining technology," *Proceedings of the SPIE*, vol. 2641, pp. 41-8, 1995.

[9] MCNC Electronics Tech. Div., 3021 Cornwallis Road, Research Trangle Park, North Carolina (http://mems.mcnc.org).

[10] W.C.Young, *Roark's Formulas for Stress & Strain*, 6th ed., McGraw-Hill Inc., 1989.

[11] P. B. Chu, P. R. Nelson, M. L. Tachiki, K. S.J . Pister, "Dynamics of polysilicon parallel-plate electrostatic actuators," *Sensors and Actuators A*, vol. A52, no. 1-3, pp. 216-220, 1996.